ChemComm

# Direct Photocatalytic C–H Functionalization Mediated by a Molybdenum Dioxo Complex



| | |
|---|---|
| Journal: | *ChemComm* |
| Manuscript ID | CC-COM-04-2024-001789.R1 |
| Article Type: | Communication |
| | |

College of Science
Department of Chemistry

## Data Availability Statement

The data supporting this article have been included as part of the Supplementary Information.

642 Choppin Hall • Baton Rouge, LA • 70803 • P 225-578-7900 • F 225-578-3458

COMMUNICATION

# Direct Photocatalytic C–H Functionalization Mediated by a Molybdenum Dioxo Complex

Received 00th January 20xx,
Accepted 00th January 20xx

DOI: 10.1039/x0xx00000x

Courtney L. Baumberger[a], Victoria Z. Valley,[a] and Matthew B. Chambers*[a]

**Direct Photocatalytic C–H activation mediated by $MoO_2Cl_2$(bpy-$^t$Bu), a unique photoactive metal oxo, is presented. The limiting step, reoxidation to the Mo dioxo, is evaluated and proposed to occur via a key $Cl^-$ loss event. Photocatalyst degradation occurs upon substitution of bpy-$^t$Bu with $H_2O$ generated during catalysis.**

Selective and efficient C–H functionalization of hydrocarbons remains a significant scientific challenge within chemical synthesis.[1–3] Commodity chemicals are commonly derived from petrochemical and biomass resources, including small alkanes, alkenes, arenes, and alcohols.[4–6] Synthetic methodologies rely on installing functional groups to activate specific sites thermodynamically or directing groups to promote sites kinetically.[7–10] Such strategies require additional steps that are not broadly applicable to arrays of synthetic targets. Thus, the direct activation and functionalization of C–H bonds has remained a stated "Holy Grail".[11,12]

Factors inhibiting direct C–H activation include the thermodynamic strength of C–H bonds (80-115 kcal/mol) and the kinetic inertness. C–H activation via a $2e^-$ oxidative addition pathway requires access to the sterically hindered σ* orbital of the C–H bond resulting in large activation barriers.[11,13–15] Biological systems and many synthetic catalysts instead activate C–H bonds by hydrogen atom transfer (HAT).[16–19] This pathway still has many drawbacks, including the fact that the H-atom acceptor must make a stronger bond to the H-atom than that of carbon (thermodynamic challenge). The activated substrate also possesses a radical prone to other reactions and decomposition (kinetic challenge).

Photocatalysis can be leveraged as a powerful strategy as it utilizes highly destabilized electronic excited states generated with light to overcome the thermodynamic challenges.[20–22] In particular, direct photocatalytic HAT is a subclass of this reaction in which the HAT is triggered directly from an excited state as opposed to a separated catalyst being oxidized by a photosensitizer.[20] The most common photocatalysts capable of mediating direct HAT include organic ketones that, upon excitation, generate an *O*-centred radical via an oxygen-to-metal charge transfer that accepts the H-atom.[20,23] The majority of direct HAT photocatalysts maintain the organic ketone motif but vary the nature of the conjugation and functionalization of the compound.[20] There are limited examples of inorganic-based photocatalysts, including decatunstages,[24] uranyls,[25,26] and antimony oxo porphyrins[27,28]. These photocatalysts maintain the O–X multiple bond motif (X=W, U, or Sb). They are proposed to react via an excited state with a radical generated via an O-to-X atom charge transfer to poise the oxygen to accept an H atom.

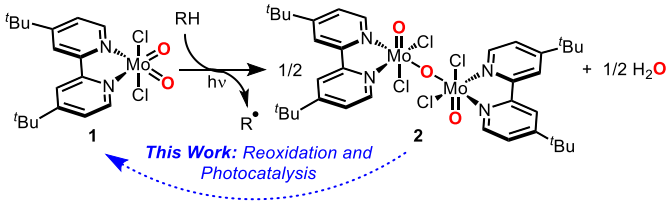


**Scheme 1** Scope of this work in achieving direct photocatalytic C–H activation.

Despite transition metal oxo complexes being ubiquitous H-atom acceptors,[29] there are no discrete examples of monometallic transition metal oxo being employed as photocatalysts for direct HAT. Seminal contributions by Fukuzumi,[30,31] Mayer,[32] Maverick,[33] and others have reported on excited state reactivity patterns of metal oxos. Still, there remains a dearth of transition metal-based photocatalysts for direct HAT and hydrocarbon functionalization.

Recently, we have reported a Mo dioxo platform $MoO_2Cl_2$(bpy-$^t$Bu), **1**, (bpy-$^t$Bu is 4,4′-*tert*butyl-2,2′bipyridine) that, upon exposure to 365 nm light, is capable of activating C–H bonds via a net HAT process.[34] Through a series of synthetic variations at the monodentate anionic position (Cl within **1**) we

[a] *Department of Chemistry, Louisiana State University, Baton Rouge, LA 70803-1804, United States. Email: chambers @lsu.edu*

Electronic Supplementary Information (ESI) available: full experimental details, NMR and UV-vis spectra, and catalytic data. See DOI: 10.1039/x0xx00000x

have collected evidence for a bpy-to-metal charge transfer being critical for the bond activation process.[35] Herein, we report the ability of **1** to achieve photocatalytic reactions from this system (Scheme 1). This work represents a rare photocatalyst for direct HAT based on a monometallic transition metal complex. It also is a unique photocatalyst for direct HAT that is not proposed to operate via the generation of an oxygen radical through an oxygen-based charge transfer but rather through an ancillary ligand-to-metal charge transfer (essentially reducing the metal without influencing the valency of the oxo). This stands to open opportunities to design HAT photocatalysts in which the basicity of the oxo is varied in the excited state to facilitate the H-atom accepting ability of the oxo during stepwise or asynchronous HAT reactions.[16,36]

Upon the stoichiometric photooxidation of hydrocarbon substrates by **1**, the Mo-containing product is the bimetallic complex $[MoOCl_2(bpy\text{-}^tBu)]_2O$, **2**. The ability to achieve catalysis requires the oxidation of bimetallic **2** to the starting dioxo complex **1** under conditions compatible with the underlying photochemistry. Most critically, this necessitates the terminal chemical oxidant to be photostable upon exposure to 365 nm light. Cerium (IV) ammonium nitrate, CAN, in the presence of advantageous $H_2O$, was previously observed to perform this oxidation, but CAN is unstable in the presence of 365 nm light.[34] Other related Mo(VI) dioxo systems can be generated through oxygen atom transfer (OAT) using reagents such as DMSO. However, **1** is unstable in excess DMSO as a substitution reaction is observed with the bpy-$^t$Bu ligand (Figure S34).

We initially surveyed a series of chemical oxidants to identify a viable candidate that could oxidize **2** into **1**, remain photostable, and not induce deleterious reactivity with either **1** or **2**. Standard oxidation attempts were performed in acetonitrile, ACN, at room temperature using a 3:1 ratio of oxidant to **2.** Oxidation was observed for *tert*butylhydrogen peroxide and trimethylamine-N-oxide, but the $^1$H NMR spectra also indicated the decoordination of the bpy-$^t$Bu ligand (Fig S10-S13). Successful oxidation to **1** was observed by $^1$H NMR spectroscopy by $Li_2CO_3$ and 4-cyanopyridin-N-oxide. Still, the reaction rates were sluggish, with only small amounts of product observed over several days of stirring at room temperature (Fig S14-S17). Pyridine-N-oxide, iodosobenzene, and $KNO_3$ were all successful at efficiently regenerating **1** over the course of several hours with no ligand loss observed and no photodecomposition of the oxidants observed in separate experiments (Fig S4-S9). Further studies were limited to pyridine-N-oxide as it is soluble in ACN at relevant concentrations and allows for synthetic modifications.

During oxidation with pyridine-N-oxide, the $^1$H NMR spectra showed the expected formation of **1** with the growth of the resonance assigned to the $^t$Bu ($\delta$ 1.48 ppm in $CD_3CN$). An additional peak was also observed slightly downfield at 1.49 ppm indicating a second complex had formed. We hypothesized that this species could be the Mo dioxo cation with an outer sphere $Cl^-$, $[MoO_2Cl(solvent)(bpy\text{-}^tBu)]Cl$. We independently prepared the dioxo cation via halide abstraction from **1** with $AgPF_6$ in ACN to interrogate this. The resulting $^1$H NMR spectrum showed a new resonance for the $^t$Bu group at exactly 1.49 ppm (Fig S22). The coincidental position of this feature with the resonance observed upon oxidation of **2** to **1** agrees with the assignment that $[MoO_2Cl(bpy\text{-}^tBu)(ACN)]Cl$ is formed during the course of the reaction (Scheme 2). The outer sphere nature of the $Cl^-$ indicates that $Cl^-$ lability from **2** may be critical to the oxidation process.

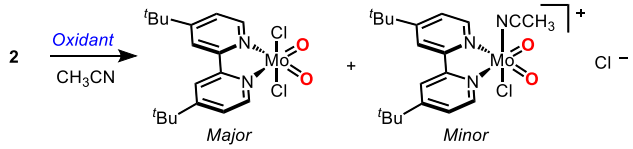


*Oxidant = PhIO, Pyridine N-oxide, $Li_2CO_3$, $KNO_3$,*

**Scheme 2**. Oxidation of **2** to a mixture of Mo(VI) dioxo products.

Measuring the initial rate of consumption of **2** by UV-vis spectroscopy while varying the concentration of pyridine-N-oxide indicates a first-order dependence on the oxidant (Fig S27). The dependence on the reaction rate with oxidant is further confirmed through synthetic variations of the pyridine-N-oxide at the 4-position where more electron-deficient oxidants are substantially slower than electron-rich oxidants, with 4-cyanopyridine-N-oxide being 50x slower than 4-methoxypyridine-N-oxide (Figure 1). A Hammett relationship between the initial rates and the 4-position functionality indicates that electron-withdrawing substituents inhibit the reaction and that the 4-cyanopyridine-N-oxide is near the limiting potential for being a viable oxidant (Figure S26).

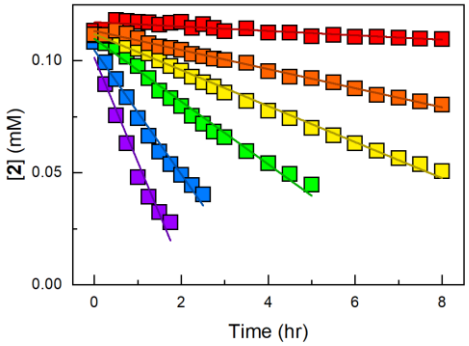


**Figure 1.** Consumption of **2** over time in the presence of various 4-R-pyridine-N-oxide. R=CN (red), Cl (yellow), H (green), $CH_3$ (blue), $OCH_3$ (purple). Orange data corresponds to 2,6 lutidine N-oxide. Photoreactions of $CH_3CN$ solutions containing 0.125 mM of **2** and 10 eq of oxidant and the bleaching of an absorption at 520 nm was monitored.

Similar studies measuring the oxidation rates while including excess free bpy-$^t$Bu of **1** in solution showed no influence on the rate. However, the inclusion of $[PPh_4]Cl$, TPPCl, in the reaction mixture resulted in a dramatic decrease in the oxidation rate, suggesting free $Cl^-$ inhibits oxidation (Figure 2). The oxidation rate initially decreases with increasing $[Cl^-]$ but then plateaus with the inclusion of ~4 equiv of $[PPh_4]Cl$ relative to **2**. Observing that higher concentrations of free $Cl^-$ does not diminish the rate further indicates that a $Cl^-$ independent pathway is operative. We propose that the oxidation can occur through two parallel processes depending on $[Cl^-]$ (Scheme 3). A preferred path occurs at low $[Cl^-]$ in which **2** initially loses an inner sphere $Cl^-$. This is followed by a rate-limiting attack of the oxidant to the open coordination site of **2**. The other pathway is

a direct attack of **2** by the oxidant. This would result in an unfavourable 7-coordinate transition state on one of the Mo centres of **2**.

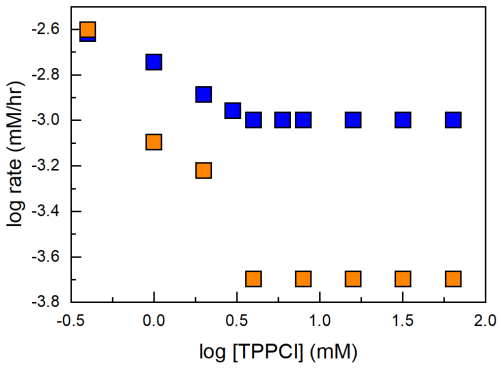


**Figure 2.** Influence of the presence of $[PPh_4]Cl$, TPPCl, on the rate of oxidation of complex **2** in $CH_3CN$ by pyridine *N*-oxide (blue) and 2,6-lutidine *N*-oxide. 1 mM of **2** in the presence of varying concentrations of TPPCl up to 40 mM.

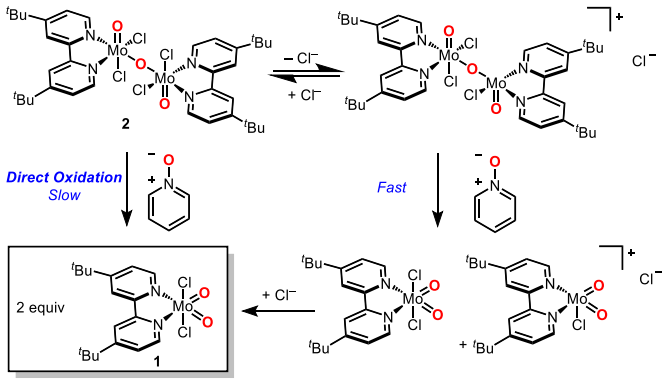


**Scheme 3.** Proposed parallel pathways for oxidation of **2** to **1.**

If a direct attack of **2** by the oxidant is viable, we hypothesized that the rate observed at the plateau region in the presence of higher [$Cl^-$] would be sensitive to the steric environment of the oxidant. A more sterically encumbered oxidant would be less likely to attack a 6-coordinate Mo center of **2**. This was observed when using 2,6-lutidine-N-oxide as the oxidant (Figure 1, orange data). Despite electron-donating methyl substituents, the rate of oxidation observed with 2,6-lutidine as the oxidant is comparable to 4-chloro-pyridine *N*-oxide and 4-cyano-pyridine *N*-oxide. An additional study monitoring the influence of $[PPh_4]Cl$ on the rate of oxidation of **2** by 2,6-lutidine-N-oxide showed that a plateau region was achieved as previously observed with pyridine-*N*-oxide, except the plateau rate (the rate proposed to be from the direct attack of **2** without chloride loss) is almost an order of magnitude less than that of pyridine-N-oxide (Figure 2). The more electron-rich nature of the dimethyl substitution pattern of 2,6-lutidine-N-oxide would electronically favour the oxidation. The decrease in plateau rate is attributed to a steric influence, which agrees with a direct attack of the oxidant occurring at higher [$Cl^-$].

With conditions established for the successful reoxidation of **2** photocatalytic assays beginning with **1** were pursued. 1 mM solutions of **1** and 100 eq of pyridine-N-oxide in ACN were photolyzed in the presence of substrates in a 5% volumetric ratio (~500 eq) with 365 nm light for 24 hours. The two substrates initially explored were 1,4-cyclohexadiene (CHD) and cyclohexene. These were chosen as we have previously reported the capacity of **1** to stoichiometrically activate CHD via HAT to yield benzene.[34] Similarly, cyclohexene can be activated via HAT to uniquely yield a bicyclic C–C coupled product via homodimerization at the allylic position.[34]

In stoichiometric photoreactions (365 nm), rapid conversion of the initially pale-yellow solution of **1** to a red solution, indicating a build-up of **2**, is observed. In the presence of 100 eq of pyridine-N-oxide and upon prolonged exposure to 365 nm light, no red solution is seen as the solution remains faintly yellow (Scheme 4). After 24 hours, GC-MS analysis confirms the photocatalytic nature of the reactions, with 6 turnover numbers (TONs) observed while using cyclohexene as a substrate and 6.5 TONs seen for CHD (Table 1). Of note, these TONs are calculated using the conventional *"TON = (mol of product)/(mol of catalyst)"* relationship, but each equivalent of product requires two C–H activations. Thus, the actual TONs for the photocatalytic C–H activation are 12-13 over 24 hours.

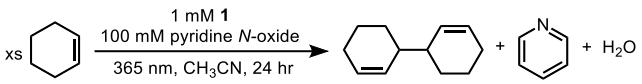


**Scheme 4.** Exemplary photocatalytic reaction using cyclohexene as substrate.

**Table 1.** Photocatalytic performance of **1**[a]

| Substrate | Initial [Oxidant] mM | Final [Product] mM | TON Product | TON C–H Activation |
|---|---|---|---|---|
| cyclohexadiene | 100 | 6.5 | 6.5 | 13 |
| | 0 | 0.5 | 0.5 | 1 |
| cyclohexene | 100 | 6.0 | 6.0 | 12 |
| | 0 | 0.4 | 0.4 | 0.8 |

[a]1 mM of **1** in a 19:1 volumetric ratio of $CH_3CN$ to substrate (~500 mM) irradiated with 365 nm light under $N_2$ for 24 hr in the presence/absence of pyridine *N*-oxide. No product yield was observed in the absence of **1.**

Unexpectedly, the product selectivity for the reaction with cyclohexene was different between the catalytic and stoichiometric reactions. We have previously found that 15% of the cyclohexene can make chlorinated products.[34] However, during the photocatalysis, no chlorination was observed, and the only product observed was the C–C coupled product. This suggests that **2** acts as a $Cl^-$ source that yields chlorinated products. During photocatalysis, there is no build-up of **2**, thus allowing greater selectivity for the homocoupled product.

Longer photolysis times did not yield greater TONs, suggesting that the photocatalyst was only active for 24 hours. The post-mortem $^1H$ NMR spectroscopic analysis indicated the decomposition of photocatalyst **1** via the loss of the bpy-$^t$Bu ligand (Fig S31). Relevant concentrations of pyridine-N-oxide or pyridine do not substitute the bpy-$^t$Bu (Figures S4 and S35). Additionally, the organic species do not displace the bpy-$^t$Bu (Figure S35). We hypothesized that the $H_2O$ generated during the reaction (Scheme 4) may initiate the decomposition of **1**. Photocatalytic assays conducted with 2 eq of $H_2O$ added to the

solution show the anticipated decrease in TONs measured (Figure 3). With cyclohexene as a substrate, the turnovers of product formation diminishes from 6 to 3 in the presence of 2 eq of $H_2O$. Additionally, the stoichiometric reoxidation of **2** by pyridine-N-oxide in the presence of 2 eq of $H_2O$ shows a greater concentration of the monocationic $[MoO_2Cl(bpy\text{-}^tBu)]^+$ species followed by growth of free bpy-$^t$Bu (Figure S32). This provides evidence for the interaction of $H_2O$ with the Mo during the reoxidation process, which may initiate a ligand substitution upon production of the cationic Mo(VI) dioxo species.

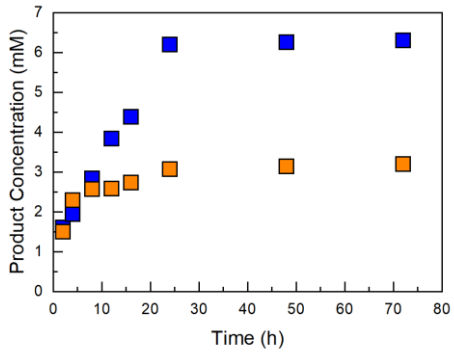


**Figure 3.** Formation of C–C coupled product from the reaction of 1 mM of **1** and 100 mM of pyridine *N*-oxide in a 19:1 volumetric ratio of $CH_3CN$:cyclohexene. Solutions irradiated with 365 nm light. Blue: 0 mM of added $H_2O$. Orange: 2 mM added $H_2O$.

In summary, we have reported the successful reoxidation of bimetallic **2** to dioxo complex **1**, the key step in closing a photocatalytic C–H activation cycle. We have proposed two parallel pathways for the reoxidation: a direct attack on a six-coordinate Mo(V) site within the bimetallic and an attack following the loss of a $Cl^-$ ligand. C–H functionalization photocatalytic assays show that over 3 TONs can be readily achieved, representing over 6 TONs of discrete C–H activation events. The rapid conversion of **2** to **1** during the photocatalysis correlated to enhanced selectivity away from chlorinated products, indicating that **2** may act as a chloride source during the reaction. Photocatalyst stability is limited by the decoordination of the bpy-$^t$Bu ligand by $H_2O$ generated during the reaction. Attempts to sequester $H_2O$ by adding molecular sieves or other drying agents ($MgSO_4$, $Na_2SO_4$, *etc*.) have proven unsuccessful to date, suggesting that a more robust ligand field is required to improve stability. In totality, these studies report one of the first examples, to our knowledge, of a monometallic transition metal oxo complex capable of mediating direct photocatalytic C–H activation via a unique LMCT excitation.[35]

We thank the National Science Foundation (Award Number 2238488), the Louisiana State Board of Regents (LEQSF(2019-22)-RD-A-03), and the ACS Petroleum Research Fund (60845-DNI3) for financial support.

## Conflicts of interest

There are no conflicts to declare.

## Notes and references

1 J. A. Labinger and J. E. Bercaw, *Nature*, 2002, **417**, 507–514.
2 J. F. Hartwig and M. A. Larsen, *ACS Cent. Sci*, 2016, **2**, 281–292.
3 M. C. White, *Science*, 2012, **335**, 807–809.
4 H. Danner and R. Braun, *Chem. Soc. Rev.*, 1999, **28**, 395–405.
5 C. H. Christensen, J. Rass-Hansen, C. C. Marsden, E. Taarning and K. Egeblad, *ChemSusChem*, 2008, **1**, 283–289.
6 P. N. R. Vennestrøm, C. M. Osmundsen, C. H. Christensen and E. Taarning, *Angew. Chem. Int. Ed.*, 2011, **50**, 10502–10509.
7 T. W. Lyons and M. S. Sanford *Chem. Rev.* 2010, **110** 1147–1169.
8 G. Rouquet and N. Chatani, *Angew. Chem. Int. Ed.*, 2013, **52**, 11726–11743.
9 J. Yamaguchi, A. D. Yamaguchi, K. Itami, J. A. Labinger and J. E. Bercaw, *Angew. Chem. Int. Ed.*, 2012, **51**, 8960–9009.
10 N. H.-Douglas and D. A. Nicewicz, *Chem. Rev.*, 2022, **122**, 1925–2016.
11 R. G. Bergman, *Nature*, 2007, **446**, 391–393.
12 X. S. Xue, P. Ji, B. Zhou and J. P. Cheng, *Chem. Rev.*, 2017, **117**, 8622–8648.
13 R. H. Crabtree, *J. Chem. Soc., Dalton Trans.*, 2001, **17**, 2437–2450.
14 S. R. Golisz, T. Brent Gunnoe, W. A. Goddard, J. T. Groves and R. A. Periana, *Catal. Lett.*, 2011, **141**, 213–221.
15 A. E. Shilov and G. B. Shulpin, *Chem. Rev.*, 1997, **97**, 2879–2932.
16 A. S. Borovik, *Chem. Soc. Rev.*, 2011, **40**, 1870–1874.
17 W. N. Oloo and L. Que, *Acc. Chem. Res.*, 2015, **48**, 2612–2621.
18 B. Meunier, S. P. de Visser and S. Shaik, *Chem. Rev.*, 2004, **104**, 3947–3980.
19 M. H. Baik, M. Newcomb, R. A. Friesner and S. J. Lippard, *Chem. Rev.*, 2003, **103**, 2385–2419.
20 L. Capaldo, D. Ravelli and M. Fagnoni, *Chem. Rev.*, 2022, **122**, 1875–1924.
21 M. Fagnoni, D. Dondi, D. Ravelli and A. Albini, *Chem. Rev.*, 2007, **107**, 2725–2756.
22 L. Revathi, L. Ravindar, W. Y. Fang, K. P. Rakesh and H. L. Qin, *Adv. Synth. Catal.*, 2018, **360**, 4652–4698.
23 J. A. Dantas, J. T. M. Correia, M. W. Paixão and A. G. Corrêa, *ChemPhotoChem*, 2019, **3**, 506–520.
24 D. Ravelli, S. Protti and M. Fagnoni, *Acc. Chem. Res.*, 2016, **49**, 2232–2242.
25 B. E. Cowie, J. M. Purkis, J. Austin, J. B. Love and P. L. Arnold, *Chem. Rev.*, 2019, **119**, 10595–10637.
26 Y. Li, J. Su, E. Mitchell, G. Q. Zhang and J. Li, *Sci. China Chem.*, 2013, **56**, 1671–1681.
27 L. Capaldo, M. Ertl, M. Fagnoni, G. Knör, D. Ravelli, *ACS Catal.*, 2020, **10**, 9057–9064.
28 T. Shiragami, J. Matsumoto, H. Inoue and M. Yasuda, *J. Photochem. Photobiol. C*, 2005, **6**, 227–248.
29 A. Gunay and K. H. Theopold, *Chem. Rev.*, 2010, **110**, 1060–1081.
30 C. Saracini, S. Fukuzumi, Y. M. Lee and W. Nam, *Dalton Trans.*, 2018, **47**, 16019–16026.
31 T. Kojima, K. Nakayama, M. Sakaguchi, T. Ogura, K. Ohkubo and S. Fukuzumi, *J. Am. Chem. Soc.*, 2011, **133**, 17901–17911.
32 S. N. Brown and J. M. Mayer, *Organometallics*, 1995, **14**, 2951–2960.
33 R. A. Isovitsch, J. G. May, F. R. Fronczek and A. W. Maverick, *Polyhedron*, 2000, **19**, 1437–1446.
34 S. Fosshat, S. D. M. Siddhiaratchi, C. L. Baumberger, V. R. Ortiz, F. R. Fronczek and M. B. Chambers, *J. Am. Chem. Soc.*, 2022, **144**, 20472–20483.
35 S. Fosshat, F. R. Fronczek and M. B. Chambers, *Chem. – Eur. J.*, *2023*, **29**, e202300486.
36 J. M. Mayer, Acc. Chem. Res., 2011, **44**, 36–46.